

Selective Kainate Receptor (GluK1) Ligands Structurally Based upon 1*H*-Cyclopentapyrimidin-2,4(1*H*,3*H*)-dione: Synthesis, Molecular Modeling, and Pharmacological and Biostructural Characterization[†]

Raminta Venskutonytė,^{‡,§} Stefania Butini,^{*,||,⊥} Salvatore Sanna Coccone,^{||,⊥} Sandra Gemma,^{||,⊥} Margherita Brindisi,^{||,⊥} Vinod Kumar,^{||,⊥} Egeria Guarino,^{||,⊥} Samuele Maramai,^{||,⊥} Salvatore Valenti,^{||,⊥} Ahmad Amir,[‡] Elena Antón Valadés,[‡] Karla Frydenvang,[§] Jette S. Kastrop,[§] Ettore Novellino,^{||,⊥} Giuseppe Campiani,^{||,⊥} and Darryl S. Pickering[‡]

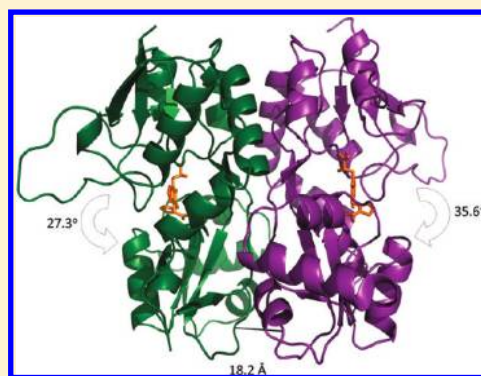
[‡]Department of Pharmacology and Pharmacotherapy and [§]Department of Medicinal Chemistry, Faculty of Pharmaceutical Sciences, University of Copenhagen, Universitetsparken 2, Copenhagen DK-2100, Denmark

^{||}Dipartimento Farmaco Chimico Tecnologico and [⊥]European Research Centre for Drug Discovery and Development (NatSynDrugs), Università degli Studi di Siena, Via Aldo Moro, 53100 Siena, Italy

[†]Dipartimento di Chimica Farmaceutica e Tossicologica, Università di Napoli Federico II, via D. Montesano 49, 80131 Napoli, Italy

S Supporting Information

ABSTRACT: The physiological function of kainate receptors (GluK1–GluK5) in the central nervous system is not fully understood yet. With the aim of developing potent and selective GluK1 ligands, we have synthesized a series of new thiophene-based GluK1 agonists (6a–c) and antagonists (7a–d). Pharmacological evaluation revealed that they are selective for the GluK1 subunit, with 7b being the most subtype-selective ligand reported to date (GluK1 vs GluK3). The antagonist 7a was cocrystallized with the GluK1 ligand binding domain, and an X-ray crystallographic analysis revealed the largest flexibility in GluK1 ligand binding domain opening upon binding of a ligand seen to date. The results provide new insights into the molecular mechanism of GluK1 receptor ligand binding and pave the way to the development of new tool compounds for studying kainate receptor function.



INTRODUCTION

Glutamate (Glu) is the main excitatory neurotransmitter in vertebrate brain and spinal cord. It is important for neurodevelopment but can also be involved in neurodegenerative processes. Its actions in the brain are mediated through excitatory amino acid transporters and metabotropic and ionotropic Glu receptors (iGluRs), which facilitate excitatory synaptic transmission upon binding of Glu.¹ Kainate receptors (KARs) belong to the family of iGluR tetrameric ligand-gated ion channels, which also consists of the (*S*)-2-amino-3-(5-methyl-3-hydroxyisoxazol-4-yl)propanoic acid (AMPA) and *N*-methyl-*D*-aspartate (NMDA) receptor subfamilies. Five KAR subunits have been identified (GluK1–5), and all except GluK4 and GluK5 can form homomeric functional channels in vitro. All the KAR subunits can combine with each other in vitro to form heteromeric receptors,^{2,3} likely in a dimer-of-dimers topology as for AMPARs and NMDARs.⁴ KARs are distributed in various areas of the central nervous system (CNS). They have been extensively studied in hippocampus and are localized on both pre- and postsynaptic cell membranes contributing to fast excitatory signaling and synaptic plasticity. KARs are expressed in cortex, amygdala, retina, striatum, hypothalamus, cerebellum, dorsal root ganglia (DRG), and spinal cord.⁵ The

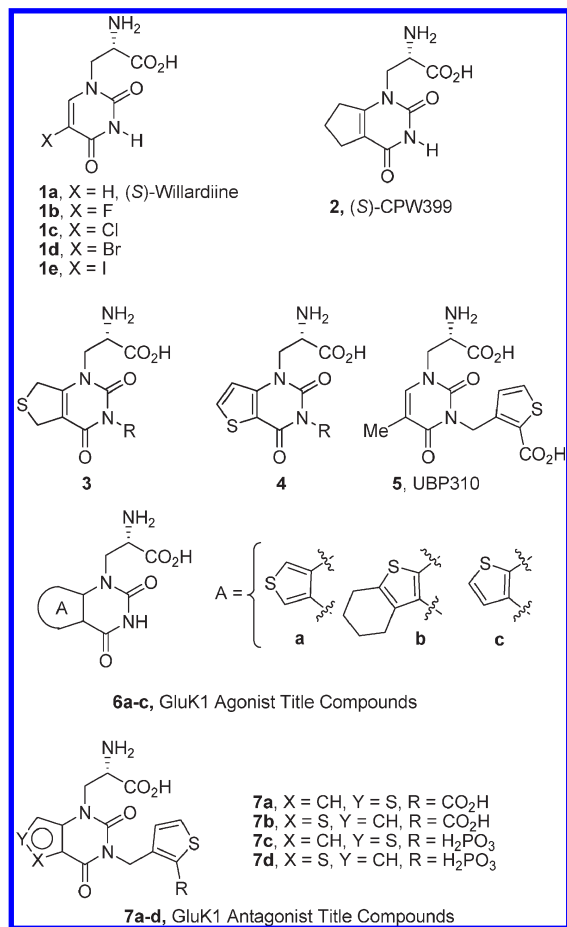
normal physiological function of these receptors is not fully understood yet although they are implicated in various neurological diseases such as depression, pain, neurodegeneration, and epilepsy.^{6,7} The GluK1 subunit is predominantly associated to pain pathways, as shown in different areas of CNS, and was found to be a key subunit in DRG neurons which are associated with primary afferents for nociceptive transmission to spinal cord.^{5,8,9} The involvement of GluK1 in pain signaling was demonstrated through the use of GluK1 competitive antagonists, which were found efficacious in animal models of persistent pain and migraine.⁹ Nevertheless the GluK1 subunit is also associated with epilepsy. KARs can affect γ -aminobutyric acid (GABA) release;² in fact, kainate induces epileptic conditions in vivo, probably due to overactivation of KARs resulting in reduction of GABA. It was also shown that GluK1 antagonists successfully eliminated epilepsy in animal models and prevented seizure initiation.¹⁰

To develop novel potent and selective KAR ligands and to implement structure–activity relationships (SARs), several compounds binding to the iGluRs have been described in the past

Received: April 6, 2011

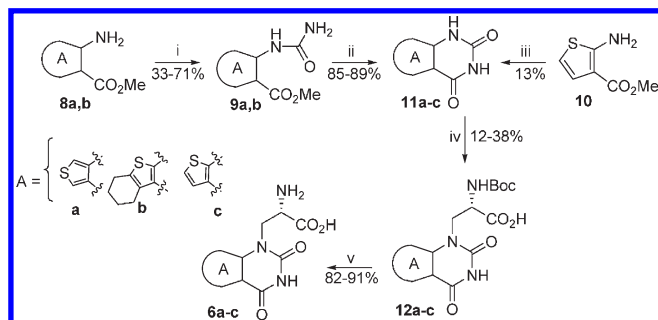
Published: May 29, 2011

Chart 1. Reference and Title Compounds

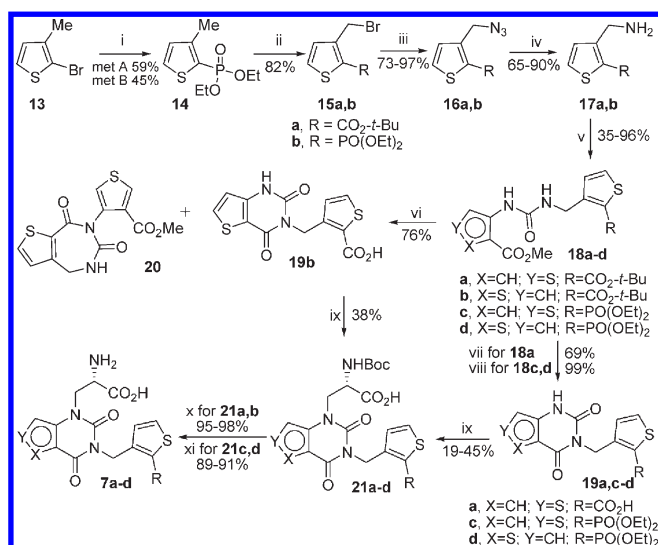


decade and have been pharmacologically and biostructurally characterized.¹¹ In fact, X-ray crystal structures of the ligand binding domain (LBD) of GluK1 and GluK2 subtypes have been solved, and several 3D structures of GluK1 LBD in complex with various ligands are available. Even though numerous molecular determinants for ligand affinity have been identified, complexes with new ligands are still providing information on receptor/ligand interactions, and there is so far much to be understood about the molecular determinants governing agonism and antagonism of KARs.

The natural product willardiine (**1a**, Chart 1), an AMPAR partial agonist, has been extensively used as a lead structure to design novel compounds targeting AMPARs and KARs. Various modifications of **1a** have been made, including 5-halo-substituted compounds (**1b–e**), some of which showed higher affinity and selectivity toward AMPARs (**1b**). While **1a** itself lacks appreciable affinity for KARs, these halo-analogues were shown to bind KARs to different extents. In addition, huge differences in affinity toward GluK1 of different halo-willardiines were shown, highlighting the sensitivity of this receptor to small changes in the ligand's structure.¹² A series of N³-substituted analogues of **1a** (the UBP compounds) were found to be potent and selective KAR antagonists at GluK1.^{13–15} (S)-1-(2-Amino-2-carboxyethyl)-6,7-dihydro-1H-cyclopenta[*d*]pyrimidin-2,4(1*H*,3*H*)dione ((S)-CPW399, **2**) is a bicyclic analogue of **1a** that was found to be a potent and subtype-selective AMPAR partial agonist which also displayed nanomolar affinity toward GluK1.¹⁶ Rational modification

Scheme 1. Synthesis of the Agonists 6a–c^a

^a Reagents and conditions: (i) triphosgene, toluene, reflux, 3 h; then NH₃ conc, EtOH, rt, 18 h; (ii) MeONa, MeOH, rt, 4 h; (iii) NaOCN, AcOH/H₂O, 5 h, rt; (iv) NaH, DMF, rt 1 h, then at –65 °C (S)-3-[(*tert*-butoxycarbonyl)amino]oxetan-2-one, rt, 18 h; (v) TFA, DCM, rt, 3 h.

Scheme 2. Synthesis of the Antagonists 7a–d^a

^a Reagents and conditions: (i) method A, Mg, THF, reflux; then diethyl chlorophosphate, THF, reflux, 2 h; method B; NiCl₂, triethyl phosphite, 160 °C, 18 h; (ii) NBS, AIBN, CCl₄, reflux, 4 h; (iii) NaN₃, DMF, 110 °C, 2 h; (iv) H₂, Pd/C, MeOH, rt, 2 h; (v) **8a** (for **18a** and **18c**) or methyl 2-aminothiophene-3-carboxylate (for **18b** and **18d**), phosgene, then **17a/b**, toluene, reflux, 3 h; (vi) **18b**, *tert*-BuONa, THF, rt, 1 h; (vii) TFA, DCM, rt; then NaOH, MeOH, reflux, 1 h; (viii) EtONa, EtOH, rt; (ix) NaH, DMF, rt 1 h, then at –65 °C (S)-3-[(*tert*-butoxycarbonyl)amino]oxetan-2-one, rt, 18 h; (x) TFA, DCM, rt, 3 h; (xi) Me₃SiBr, DCM, rt;

of the structure of **2** already allowed us to identify potent and selective GluK1 ligands (**3** and **4**) endowed with antagonist activity at cloned receptors.¹⁷

On the basis of our previous experience, and with the aim of developing potent and selective GluK1 agonists/antagonists, we decided to investigate the bicyclic scaffold of **3** and **4** to identify novel GluK1 ligands (**6a–c**, **7a–d**). While potency was improved by introduction of a sulfur-bridged atom on the uracil system, the insertion of an acidic moiety at N³ converted the agonism to full antagonism, similarly to **5**. We here present the synthesis and the pharmacological investigation of analogues of **3**

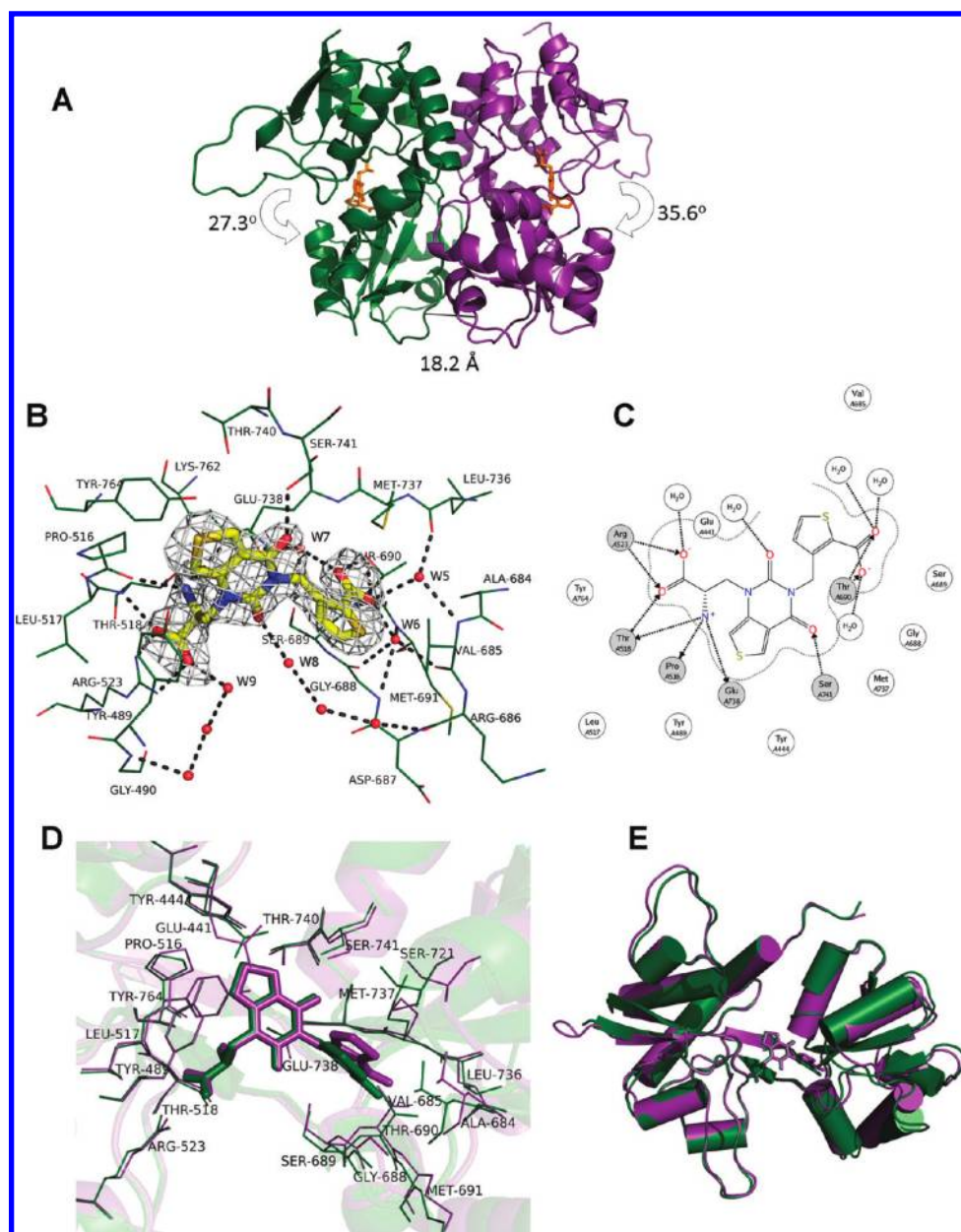


Figure 1. Crystal structure of the ligand binding domain of GluK1 in complex with the antagonist 7a. (A) Dimeric structure of GluK1 LBD with one 7a molecule bound in each protein molecule. 7a is shown in stick representation and colored orange. The domain openings and linker-linker distances are indicated. The linker region is where the amino acid sequence continues into the transmembrane ion channel pore. GluK1 molA is shown in green and molB in purple. (B) Zoom on the binding pocket with 7a in atom type stick representation. The $F_o - F_c$ OMIT electron density map (contoured at 3σ level) is shown of 7a (molA) as well as potential hydrogen bonding interactions from 7a to GluK1 residues within 3.3 Å as dashed lines. (C) 2D ligand-receptor interaction plot of GluK1 LBD in complex with 7a. Contacts from ligand to receptor side chains as calculated by the program MOE²⁶ are shown as arrows. Residues forming potential hydrogen bonds to 7a are shown as gray circles, whereas other residues within 4.5 Å of 7a and water molecules are shown as white circles. (D) Zoom on binding sites of overlaid structures of molA (in green) and molB (in purple). (E) Superimposition of GluK1 molA and molB to illustrate differences in D1-D2 domain openings.

and 4, namely the agonists 6a–c and the antagonists 7a–d. Furthermore, the crystal structure of the GluK1 LBD in complex with the novel selective antagonist 7a is presented.

CHEMISTRY

Scheme 1 describes the synthesis of the designed agonists (6a–c), and Scheme 2 describes the synthesis of the designed antagonists (7a–d).

The key step in synthesis of 6a–c (Scheme 1) is the formation of the pyrimidindione systems 11a–c. The amines 8a,b were reacted with triphosgene and immediately treated with concentrated aqueous ammonia to furnish the ureido intermediates 9a,b.¹⁸ Treatment of 9a,b with a solution of sodium methoxide promoted their cyclization into the uracil derivatives 11a,b. This synthetic procedure was not applicable to compound 10. The pyrimidindione 11c was synthesized (according to the procedure previously reported for compound 3¹⁷) by treatment of 10 with

Table 1. Binding Affinities of 6a–c, 7a–d and Reference Compounds at Recombinant Rat iGluRs Expressed in Sf9 Cells^a

compd	K _i (nM)				GluK1 selectivity	
	GluA2	GluK1	GluK2	GluK3	GluA2/GluK1	GluK3/GluK1
2 ^b	223 ± 12	44 ± 4	>1000000	5090 ± 1190	5	116
3 ^b	80 ± 13	5.20 ± 0.28	>1000000	3250 ± 300	15	625
4 ^b	112 ± 10	5.29 ± 0.66	>1000000	3650 ± 570	21	690
5	>100000 ^c	10 ^c	>100000 ^c	23 ^d	>10000	2
6a	465 ± 2	3.90 ± 0.37	>1000000	1022 ± 253	119	262
6b	>100000	3673 ± 551	>1000000	72300 ± 23300	>27	20
6c	503 ± 69	5.89 ± 0.59	>1000000	4750 ± 810	85	806
7a	72900 ± 14600	157 ± 22	98950 ± 22380	7450 ± 300	464	53
7b	107700 ± 8800	567 ± 114	>1000000	53750 ± 3370	190	95
7c	>1000000	15090 ± 1940	>1000000	>1000000	>66	>66
7d	>100000	11970 ± 2010	>1000000	>1000000	>8	>84

^a Reported data are mean ± SEM values of at least three experiments conducted in triplicate at 12–16 ligand concentrations. Hill coefficients of ligands were not different from unity (data not shown). ^b Data for GluA2, GluK1 and GluK2 from ref.¹⁷ ^c From ref.¹⁵ ^d From ref.³⁰

sodium isocyanate in water/acetic acid solution.¹⁹ The introduction of the amino acid chain was performed by treating the sodium salt of **11a–c** with the *N*-Boc-protected L-serine lactone.²⁰ To minimize *N*³-alkylation, and because the *N*¹ of compounds **11a–c** is more acidic than the *N*³, we performed the lactone addition at –65 °C regioselectively obtaining **12a,c**, while in the case of **11b** partial *N*¹,*N*³-dialkylation occurred. After deprotection of the amino group, **6a–c** were purified using a Dowex cationic resin.

For the synthesis of the antagonists **7a–d** (Scheme 2), the ureidic intermediates (**18a–d**) were obtained by reacting amines **17a,b** with the appropriate isocyanates or amines in the presence of triphosgene. The synthesis of amine **17a,b** starts from bromides **15a** and **15b**.^{14,15} Bromide **15b** was prepared from **13**, which was converted into the key phosphonic ester **14**. To accomplish this latter conversion, we employed two different protocols. The standard Tavs' method^{21,22} (method B of the Experimental Procedures, see Scheme 2) gave compound **14** in 45% yield. However, due to the drawbacks of this procedure (such as use of high temperatures, strongly smelling triethyl and trimethylphosphite and toxic NiCl₂ reactants, coupled to the risk of explosions) a specific synthetic route was developed which exploits the reaction of Grignard reagents with electrophilic species of phosphorus, such as alkyl chlorophosphates (method A of the Experimental Procedures).²³ Following this latter protocol, we obtained **14** in 59% yield, better than following classical method B. Ester **14** was then subjected to a radical bromination reaction (**15b**). Bromides **15a,b** were reacted with sodium azide for obtaining **16a,b**, which were converted into the corresponding amines **17a, b** by means of a palladium catalyzed hydrogenation reaction. Because of the presence of the thiophene ring, a known sulfur-based catalyst poison, the reaction successfully proceeded only after multiple additions of the catalyst. Exposure of **17a,b** to the appropriate amine and phosgene or isocyanates furnished intermediates **18a–d**. Compound **18a** was then treated with TFA and subsequently with sodium hydroxide to furnish **19a**. Interestingly, treatment of **18b** with sodium *tert*-butoxide, followed by an acidic workup, also allowed the hydrolysis of the *tert*-butyl ester, but the use of a strong base triggered a competition between the two ureidic nitrogens and, together with the desired compound **19b**, **20** was also obtained. Cyclization of ureas **18c,d**

phosphono esters **19c,d** was carried out using sodium ethoxide (no phosphoro-amide bond formation was detected). Compounds **7a,d** were then obtained after *N*-alkylation of **19a–d**, followed by acidic deprotection of **21a,b** or treatment of **21c,d** with trimethylsilyl bromide, which allowed simultaneous hydrolysis of the phosphonate ester and removal of the Boc protecting group.

RESULTS AND DISCUSSION

X-ray Structure Determination of 7a in Complex with GluK1 LBD. As **7a** was the most potent antagonist at GluK1 of the new series (see below), we decided to crystallize this compound with the rat GluK1-S1S2 construct (99% sequence identity to human GluK1 LBD), comprising its LBD in order to establish its interactions with the receptor. The complex crystallized in space group *P*2₁2₁2₁ and crystallographic data were obtained at 2.5 Å resolution (Table 1 Supporting Information). Two molecules (molA and molB) were found in the asymmetric unit of the crystal (Figure 1A), forming a conventional dimer. The electron density of **7a** is well-defined in the ligand binding site (Figure 1B), allowing its unambiguous positioning and identification of receptor–ligand interactions. **7a** interacts with both domains D1 and D2 via H-bonds, electrostatic interactions, van der Waals (vdW) interactions, and through water mediated hydrogen bonds.

Molecular interactions between **7a** and D1 of GluK1 LBD are very similar in both molecules of the dimer, and they resemble the common contacts made by Glu and most of the other GluK1 ligands. As shown in Figure 1B, the α-carboxyl group of **7a** forms an ion pair interaction with the Arg523 side chain and an H-bond to the Thr518 backbone nitrogen atom. The α-amino group of **7a** makes H-bonds with the carbonyl oxygen of Pro516 and with the side chains of Thr518 within D1 and Glu738 within D2. Thr518 was shown to be crucial for binding of the willardiine analogue antagonist **5** in site-directed mutagenesis studies²⁴ and, as we see here, the similar mode of binding of **7a** results in the same ligand contacts. The importance of the Thr518 interaction with the ligand may also explain the lack of affinity of **7a** toward GluK2, as this subtype has Ala in the corresponding position. The fused thiophene ring of **7a** establishes vdW

interactions (within 4 Å) with Glu441, Tyr444, Tyr489, Pro516, and Tyr764 in D1 and with Ser741 in D2.

The thienylmethyl at the N³ atom of the uracil ring of **7a** reaches out toward domain D2, thereby preventing closure of the GluK1 LBD. It is noteworthy that the positioning of this moiety in **7a** within the LBD differs between molA and molB (Figure 1C). In molA, the distal thiophene ring is located deeper in the binding cleft than in molB, resulting in slightly different interactions between **7a** and the D2 residues (Table 2 Supporting Information). This flexibility in the location of the distal thiophene ring has been previously observed also for UBP compounds upon binding to the GluK1 LBD.²⁵

A much more dramatic effect is seen on LBD domain opening. Analyzing the degree of domain opening compared to the glutamate bound structure (PDB code 2F36), molA was found to have an open conformation of 27.3°, whereas molB adopts a hyperextended conformation of 35.6° (Figure 1A and 1D). The domain opening in molA is comparable to that seen in the GluK1:5 complex (29.3°), but to our knowledge the domain opening in molB is the largest domain opening seen in any GluK1 LBD structure and also the largest difference (8.3°) seen between the two molecules forming the biologically relevant dimer. These observations show that domain movements can vary to a large extent even upon binding of the same compound. However, the linker–linker distance measured between two Ile668 residues was 18.2 Å (Figure 1A) and is comparable to those observed in GluK1:UBP compound complexes.^{25,27} This suggests that D2 movements within the GluK1 dimer can vary but the linker–linker distance is specific for antagonists and full and partial agonists.

Glu738 was seen to form an important ionic contact with the α-amino group of **7a**. It has previously been speculated that this interaction requires a certain amount of domain closure to occur.²⁵ In our structure, this is definitely not the case as the ion pair interaction between Glu738 and the α-amino group of **7a** is seen in both molA and molB despite the large difference in domain arrangement. Therefore, the Glu738 interaction with the α-amino groups of bound ligands cannot depend solely on the degree of domain closure but more likely is due to a whole complex set of movements in the protein molecule, once again indicating conformational flexibility.

Pharmacology, Structure–Affinity Relationships and Molecular Modeling Studies. *GluK1 Agonists.* Upon the basis of the previously reported¹⁷ pharmacological profile of the (*S*)-2 thieno-analogues **3** and **4**, two additional thieno-compounds were synthesized, **6a** and **6c**, where the sulfur-bridged atom was introduced at different positions within the thienopyrimidindione system. The radioligand binding affinities of **3**, **4**, **6a**, and **6c** at GluK1 were similar ($P > 0.05$, one-way ANOVA), indicating that, while the presence of sulfur in the ring structure enhances affinity compared to (*S*)-2, the position of the sulfur is not critical (Table 1). This is in agreement with a large binding cavity in the closed form of the GluK1 LBD,²⁸ favoring the bulkier sulfur containing compounds. Unfortunately, it has not been possible yet to crystallize one of these thieno-compounds in the GluK1 LBD, so the exact nature of the interactions leading to an increased binding affinity has not been experimentally determined.

To elucidate the binding mode of these compounds within the LBD and to rationalize the selectivity profile, docking studies were performed with both GluA2 and GluK1 subunits. All the compounds docked inside the GluA2 LBD construct share very similar binding poses, and all thieno-analogues are capable of

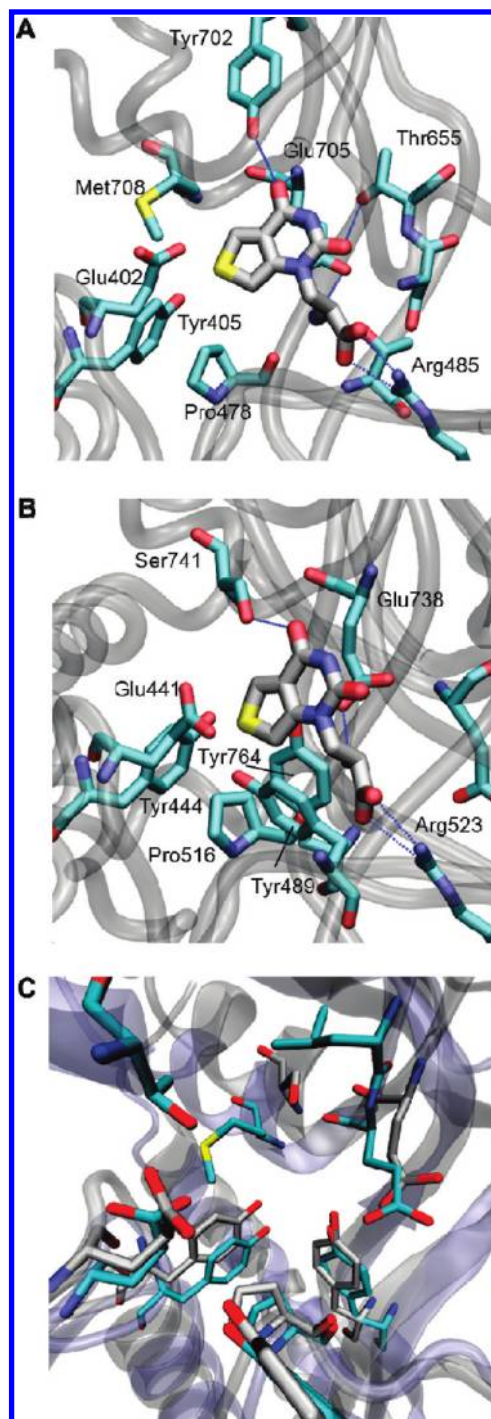


Figure 2. Binding modes of compound **6a** docked into GluA2 LBD (A) and into GluK1 LBD (B), respectively. Superimposition of GluA2 LBD and GluK1 LBD (C). The carbon atoms of the main residues are represented as cyan (GluA2 LBD) and silver (GluK1 LBD). The main binding site residues are represented as atom type colored sticks. The potential hydrogen bond interactions are indicated as blue dashed lines between donor and acceptor atoms (A,B).

establishing hydrophobic and H-bond interactions similar to those already observed in the crystal structure of (*S*)-2 in complex with GluA2 LBD²⁹ (Figure 2A, see Figure 1A of the Supporting Information for stereo view). This result is in

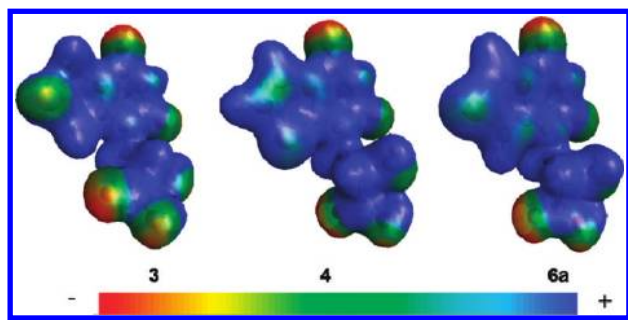


Figure 3. Electrostatic potential mapped on the electron density surface of **3**, **4**, and **6a**. The calculations were computed at Hartree–Fock level of theory and using 6-31G* as basis set. The scale of the electrostatic potential is negative (red) to positive (blue).

agreement with the binding data exhibited by these compounds for GluA2 (Table 1). However, a similar ligand binding mode was also observed when docking experiments were performed in the GluK1 LBD binding cleft (Figure 2B, see Figure 1B Supporting Information for stereo view).

Binding studies proved that **6a** is one of the most potent GluK1 agonists known to date with a $K_i = 3.9$ nM and a GluK1 selectivity of 119-fold. This compound was found to be more selective than **3**, **4**, and **6c**. A factor that may explain the GluK1 selectivity of all these compounds is the steric hindrance offered by Met708 in the GluA2 LBD. Indeed, in the absence of this residue, as in the GluK1 receptor cleft (see Figure 2C), a larger void is present where the bulkier thieno bicyclic systems can better fit and orientate in order to find the favorable interactions.

The Met708 *S*-methyl group could establish a polar interaction with a negative dipole. In line with this hypothesis, we can explain the different potency at GluA2 of **4**, **6a**, and **6c** (K_i at GluA2 = 112–503 nM, Table 1) with respect to the nonaromatic **3** (K_i at GluA2 = 80 nM). The electrostatic potential maps of **3**, **4**, and **6a** were generated by means of an *ab initio* method (Figure 3). Theoretically calculated charge distributions of the compounds depicted in Figure 3 indicated the dihydrothieno-analogue **3** as having the more electron rich sulfur-bridged atom. Because the higher electron density found for **3** cannot be delocalized on an aromatic system as in **4**, **3** may establish a more favorable interaction with Met708. This may explain the higher affinity of **3** for GluA2 with respect to the aromatic compounds **4** and **6a**. Accordingly, **6a** is the most selective compound of the series toward the GluK1 subunit (GluA2/GluK1 = 119). For the same reason, we can explain the lower affinity of **2** for GluA2 ($K_i = 223$ nM).

In this series, the extension of the bicyclic system of **4** by a fused cyclohexane group (**6b**) was clearly unfavorable, as a loss of affinity of 700-fold was observed. Most likely this is the result of steric clashes with residues in the vicinity of Pro516 of the bulky cyclohexyl group.

The previously reported thieno-analogues (**3** and **4**) were found to be very weak partial agonists at wild-type homomeric GluK1(Q)_{1b} expressed in CHO-K1 mammalian cells, exhibiting extremely rapid and complete desensitization¹⁷ and, as such, behaving as functional antagonists. The functional activities of the parent compound (**2**) and its thieno-analogues were evaluated by two-electrode voltage clamp (TEVC) electrophysiology using nondesensitizing mutants of GluK1(Q)_{1b} and GluK3.³¹ In agreement with the binding data, the thieno-analogues had an

approximately 10-fold increase in potency (EC_{50}) compared to the parent compound (**2**, Table 2). Measurement of the efficacies of the thieno-analogues indicated that they are all partial agonists at the nondesensitizing GluK1 mutant (Figure 4, Table 2), while **3** and **4** had somewhat higher efficacy than **2** ($P < 0.001$, Kruskal–Wallis one-way ANOVA on Ranks with Dunn's post test). It should be mentioned that although the thieno-analogues **3** and **4** have been demonstrated to be partial agonists at wild-type GluK1,¹⁶ the new thieno-analogues **6a,c** have not been examined at wild-type receptors and therefore we cannot conclusively state that they are partial agonists at wild-type receptors. The affinity data and functional potencies indicated that all these compounds exhibited selectivity for GluK1 vs either GluA2 or GluK3, having no appreciable affinity at GluK2 (Table 1 and 2). Compound **6a** exhibited the highest KAR vs AMPAR selectivity (119, Table 1), while compound **6c** showed the highest selectivity among the KAR (GluK1 vs GluK3 = 806, Table 1). Interestingly, at the nondesensitizing GluK3 receptor, all these compounds appear as weak antagonists.

GluK1 Antagonists. In line with the objective of the present study, we also evaluated the functionalization at the N³ pyrimidinedione nitrogen with an aromatic moiety containing an additional acid group, namely a carboxyl or phosphonic group. Therefore, N³-2-carboxythien-3-ylmethyl analogues of **4** and **6a** (**7b** and **7a**) were prepared. This structural modification allowed us to convert agonists into full antagonists. **7b** and **7a** proved to be selective GluK1 ligands having very low affinity at GluA2 and GluK2 with micromolar affinity towards GluK3 (Table 1). In particular, while **7a** exhibited the highest affinity for GluK1 and the highest GluK1 vs GluA2 selectivity ratio (464), **7b** showed a higher KAR subtype-selectivity (95-fold, GluK1 vs GluK3). Therefore, to our knowledge, **7b** is the most subtype-selective KAR antagonist reported to date, more selective than **5** (Table 1). Comparing the affinity of **7a** and **7b** at GluK1, we can speculate that the higher affinity of **7b** may be due to the different position of the sulfur-bridged atom in the bicyclic scaffold. To further explore the SAR of this series of compounds and the influence of the carboxylate bioisosteric replacement, the phosphono derivatives **7d** and **7c** were prepared and tested. Compounds having a terminal carboxyl group, as **7a** and **7b**, displayed 100-fold higher affinity than the phosphono-analogues (**7d** and **7c**).

In functional TEVC studies **7b** and **7a** behaved as pure competitive antagonists at GluK1 and were, as far as could be divined, devoid of agonist activity (Figure 4, Table 2). Moreover, **7a** was seen to be an antagonist at GluA2 (1 mM (*S*)-Glu + 100 μM cyclothiazide vs 1 mM **7a** + 100 μM cyclothiazide: efficacy = 0.000, ($n = 3$)) and **7b** demonstrated to be an extremely weak partial agonist at GluA2 (1 mM (*S*)-Glu + 100 μM cyclothiazide vs 1 mM **7b** + 100 μM cyclothiazide: efficacy = 0.0053 ± 0.0014, ($n = 3$)). The calculated K_b values of **7b**, **7a**, and **5** at the nondesensitizing GluK1 and GluK3 (Table 2) are in good agreement with the K_i values determined from radioligand binding assays. In functional studies, **7a** was found more potent than **7b** at GluK1. However, we have to take into consideration the behavior of known partial agonists such as kainate, domoate, and dihydrokainate that at the nondesensitizing GluK1–3 receptors appeared as antagonists. The disulfide linkage of these mutant receptors that prevents conversion into the desensitized state³¹ perhaps also impedes normal D1–D2 domain closure such that partial agonists may then appear as antagonists.

Table 2. Potencies of Selected Compounds and Standard Ligands at Non-Desensitizing Homomeric Rat KAR Expressed in *Xenopus laevis* Oocytes^a

compd	EC ₅₀ or K _b (μM)					
	GluK1		GluK2		GluK3	
	EC ₅₀	n _H	efficacy	K _b	n _H	efficacy
2	9.87 ± 1.51 (15)	1.06 ± 0.04	0.459 ± 0.028 (15)	nd	nd	123 ± 18 (3)
3	1.56 ± 0.05 (8)	1.15 ± 0.02	0.652 ± 0.016 (6)	nd	nd	>300 (5)
4	0.719 ± 0.054 (8)	1.13 ± 0.04	0.680 ± 0.043 (8)	nd	nd	>300 (5)
6a	4.23 ± 0.41 (9)	1.03 ± 0.04	0.562 ± 0.019 (9)	nd	nd	>300 (5)
6c	3.55 ± 0.26 (10)	1.32 ± 0.06	0.562 ± 0.035 (10)	nd	nd	>300 (5)
	K _b	n _H	efficacy	K _b	n _H	efficacy
7a	0.0866 ± 0.0088 (10)	1.07 ± 0.04	0.000 (6)	159 ± 37 (4)	1.16 ± 0.02	0.000 (3)
7b	0.344 ± 0.049 (10)	1.08 ± 0.04	0.000 (3) ^b	>1000 (3)	—	0.000 (3)
5	0.019 ± 0.003 (6)	1.20 ± 0.08	0.000 (3)	207 ± 34 (5)	1.65 ± 0.10	0.000 (3)
	EC ₅₀	n _H	efficacy	EC ₅₀	n _H	efficacy
(S)-Glu	83.5 ± 9.5 (12)	1.23 ± 0.09	1.000	108 ± 9.4 (21)	0.87 ± 0.03	1.000
(2S,4R)-4-Me-Glu	0.558 ± 0.063 (7)	1.19 ± 0.04	0.991 ± 0.031 (6)	1.55 ± 0.12 (6)	0.96 ± 0.04	0.718 ± 0.022 (5)
	K _b	n _H	efficacy	K _b	n _H	efficacy
dihydrokainate	161 ± 25 (5)	1.00 ± 0.04	0.000 (3)	72 ± 9 (5)	1.17 ± 0.09	0.000 (3)
kainate	2.15 ± 0.24 (10)	1.23 ± 0.05	0.000 (3)	0.7036 ± 0.0356 (5)	1.20 ± 0.03	0.000 (3)
domoate	0.0202 ± 0.0019 (9)	1.28 ± 0.05	0.000 (3)	0.0598 ± 0.0068 (6)	1.31 ± 0.11	nd
	EC ₅₀	n _H	efficacy	EC ₅₀	n _H	efficacy
(S)-Glu	83.5 ± 9.5 (12)	1.23 ± 0.09	1.000	108 ± 9.4 (21)	0.87 ± 0.03	1.000
(2S,4R)-4-Me-Glu	0.558 ± 0.063 (7)	1.19 ± 0.04	0.991 ± 0.031 (6)	1.55 ± 0.12 (6)	0.96 ± 0.04	0.718 ± 0.022 (5)
	K _b	n _H	efficacy	K _b	n _H	efficacy
dihydrokainate	161 ± 25 (5)	1.00 ± 0.04	0.000 (3)	72 ± 9 (5)	1.17 ± 0.09	0.000 (3)
kainate	2.15 ± 0.24 (10)	1.23 ± 0.05	0.000 (3)	0.7036 ± 0.0356 (5)	1.20 ± 0.03	0.000 (3)
domoate	0.0202 ± 0.0019 (9)	1.28 ± 0.05	0.000 (3)	0.0598 ± 0.0068 (6)	1.31 ± 0.11	nd

^a Reported data are mean ± SEM values of experiments conducted in duplicate at 6–10 ligand concentrations. Number of experiments indicated in parentheses. Efficacy of 0.000 means no agonism detected at 1 mM compound. nd, not determined. ^b At 0.30 mM compound. ^c Fractional response of 2 mM (S)-Glu + 1 mM dihydrokainate vs 2 mM (S)-Glu alone. ^d Fractional response of 1 mM dihydrokainate vs 100 mM (S)-Glu alone. ^e Hill coefficient.

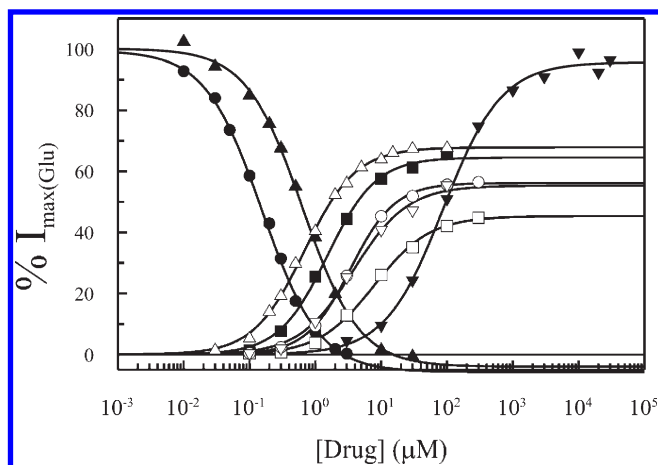


Figure 4. TEVC pharmacology of compounds at nondesensitizing GluK1 expressed in *Xenopus laevis* oocytes. Shown are mean values of pooled data from 8 to 15 concentration–response curves, conducted in duplicate. Agonist curves have been normalized to the maximal response of (S)-Glu in order to illustrate relative efficacies. Note: the lower plateau for antagonist curves drops below zero due to inhibition of the baseline oocyte current at high antagonist concentrations. Error bars on the data points have been omitted for the sake of clarity: ■, 3; ●, 7a; ▲, 7b; ▼, (S)-Glu; Δ, 4; ▽, 6a; ○, 6c; □, 2.

CONCLUSIONS

In conclusion, the kainate receptor GluK1 is one of the most studied receptor subtypes among the ionotropic glutamate receptors and has been associated with various neurological diseases. In particular, it was demonstrated to be involved in pain signaling through clinical and preclinical studies. However, more research is needed to clarify this issue by means of more selective ligands. Synthesis of novel GluK1 selective compounds is therefore important for understanding its functioning at the molecular level. Here, we present new rationally designed antagonists, based upon the structure of previous iGluRs ligands, which show GluK1 receptor selectivity. These results encourage the design of optimized ligands for the kainate receptors, which can ultimately lead to a better understanding of the role of the receptors in normal and pathological brain functions.

EXPERIMENTAL PROCEDURES

Chemistry. Reagents were purchased from Aldrich and were used as received. Reaction progress was monitored by TLC using Merck Silica Gel 60 F254 (0.040–0.063 mm) with detection by UV. Merck Silica Gel 60 (0.040–0.063 mm) was used for column chromatography. All moisture-sensitive reactions were performed under argon atmosphere using oven-dried glassware and anhydrous solvents. All the organic layers were dried using anhydrous sodium sulfate. ^1H NMR, ^{13}C NMR, and ^{31}P NMR spectra were recorded using a Varian 300 MHz spectrometer with TMS as internal standard. Splitting patterns are described as singlet (s), doublet (d), triplet (t), quartet (q), and broad (br); the value of chemical shifts (δ) are given in ppm and coupling constants (J) in hertz (Hz). ESI-MS, spectra were performed by an Agilent 1100 series LC/MSD spectrometer. Elemental analyses were performed in a Perkin-Elmer 240C elemental analyzer and the results were within $\pm 0.4\%$ of the theoretical values, unless otherwise noted. Optical activities were measured using Perkin-Elmer model 343 polarimeter. Yields refer to purified products and are not optimized. Optical rotation values were measured at rt operating at $\lambda = 589$ nm, corresponding to the sodium

D line, and were determined, using a microcell (1 mg sensitivity) containing the compound dissolved in 1 mL of the appropriate solvent.

For testing, compounds 6a–c and 7a–d were transformed in the corresponding hydrochloride salts by a standard procedure.

Methyl 4-Ureidothiophen-3-carboxylate (9a). To a solution of 8a (620 mg, 3.95 mmol) in dry toluene (15 mL), triphosgene (385 mg, 1.31 mmol) was added and the solution was refluxed for 3 h. The solvent was evaporated and to the residue, taken up with EtOH (10 mL), an EtOH saturated solution of ammonia (15 mL) was added. The resulting mixture was stirred at rt for 18 h. The solvent was evaporated, and the crude product was purified by means of flash chromatography (*n*-hexane/EtOAc 1:1) to give 9a as a white solid (yield 71%). ^1H NMR (DMSO- d_6) δ 8.88 (br s, 1H), 8.26 (d, 1H, $J = 3.6$ Hz), 7.63 (d, 1H, $J = 3.6$ Hz), 6.51 (br s, 2H), 3.82 (s, 3H). ESI-MS m/z 223 ($M + \text{Na}$) $^+$, 199 ($M - \text{H}$) $^-$.

Ethyl 2-Ureido-4,5,6,7-tetrahydrobenzo[*b*]thiophen-3-carboxylate (9b). Starting from 8b, the title compound was prepared following the same procedure used for the synthesis of 9a and was obtained as a white solid (yield 33%). ^1H NMR (DMSO- d_6) δ 10.21 (br s, 1H), 6.93 (br s, 2H), 4.23 (q, 2H, $J = 7.0$ Hz), 2.64 (m, 2H), 2.48 (m, 2H), 1.67 (m, 4H), 1.27 (t, 3H, $J = 7.0$ Hz). ESI-MS m/z 291 ($M + \text{Na}$) $^+$.

Thieno[3,4-*d*]pyrimidin-2,4-dione (11a). To a solution of NaOMe (440 mg, 8.1 mmol) in dry MeOH (10 mL) 9a (560 mg, 2.8 mmol) was added, and the resulting mixture was stirred at rt for 4 h. Then the solvent was evaporated, and the residue was dissolved in water (10 mL). The solution was cooled to 0 °C, acidified by dropwise addition of HCl 4N. The precipitate was filtered and dried in an oven at 60 °C to give 11a as a white solid (yield 89%). ^1H NMR (DMSO- d_6) δ 10.9 (br s, 2H), 8.32 (d, 1H, $J = 3.2$ Hz), 6.78 (d, 1H, $J = 3.2$ Hz). ^{13}C NMR (DMSO- d_6) δ 159.2, 151.3, 138.3, 130.8, 122.6, 103.4. ESI-MS m/z 191 ($M + \text{Na}$) $^+$.

1,2,3,4,5,6,7,8-Octahydrobenzo[4,5]thieno[2,3-*d*]pyrimidin-2,4-dione (11b). Starting from 9b, the title compound was prepared following the same procedure used for the synthesis of 11a and was obtained as a white solid (yield 85%). ^1H NMR (DMSO- d_6) δ 11.73 (br s, 1H), 10.93 (br s, 1H), 2.71 (m, 2H), 2.57 (m, 2H), 1.75–1.66 (m, 4H). ESI-MS m/z 245 ($M + \text{Na}$) $^+$.

Thieno[2,3-*d*]pyrimidin-2,4-dione (11c). A mixture of 10 (1.10 g, 7.00 mmol) with a solution of sodium cyanate (910 mg, 14 mmol) in water (15.0 mL) was added dropwise to a 50% solution of glacial acetic acid in water (30 mL). The resulting solution was stirred at rt for 5 h. The formed precipitate, collected by filtration, was dissolved in NaOH 2N (15 mL). The solution, cooled to 0 °C, was acidified with HCl 4N and the filtered solid was dried in an oven at 60 °C to give 11c as a white solid (152 mg, 13% yield). ^1H NMR (DMSO- d_6) δ 11.88 (br s, 1H), 11.11 (br s, 1H), 7.11–7.05 (m, 2H). ESI-MS m/z 191 ($M + \text{Na}$) $^+$.

(S)-1-[2'-(tert-Butoxycarbonylamino)-2'-carboxyethyl]thieno[3,4-*d*]pyrimidin-2,4-dione (12a). To a solution of 11a (487 mg, 2.9 mmol) in dry DMF (30 mL) and NaH (70 mg, 2.9 mmol) was added, and the resulting mixture was stirred for 1 h at rt. Then the formed suspension was cooled to –65 °C and a solution of (S)-3-[(tert-butoxycarbonyl)amino]oxetan-2-one (542 mg, 2.9 mmol) in dry DMF (10 mL) was added dropwise in 1 h. When the addition was completed, the mixture was allowed to reach rt and left 18 h under stirring. The solvent was evaporated and the crude product taken up in water (30.0 mL). The aqueous phase was acidified to pH 2 by addition of HCl 4N and then extracted with EtOAc. The collected organic layers were dried, filtered, and concentrated. The crude product was purified by means of flash chromatography (DCM/MeOH/AcOH, from 97:3:0.1 to 90:10:1) to give 12a as an amorphous white solid (yield 12%). ^1H NMR (CD $_3$ OD) δ 8.31 (d, 1H, $J = 3.2$ Hz), 7.17 (d, 1H, $J = 3.2$ Hz), 4.66–4.61 (m, 1H), 4.42–4.12 (m, 2H), 1.27 (s, 9H). ESI-MS m/z 354 ($M - \text{H}$) $^-$.

(S)-1-(2'-(tert-Butoxycarbonylamino)-2'-carboxyethyl)-1,2,3,4,5,6,7,8-octahydrobenzo[4,5]thieno[2,3-*d*]pyrimidin-2,4-dione (12b). Starting from 11b, the title compound was prepared following the same

procedure used for the synthesis of **12a** and was obtained as a white solid (yield 38%). $^1\text{H NMR}$ (CD_3OD) δ 4.71–3.95 (m, 3H), 2.77 (m, 2H), 2.65 (m, 2H), 1.82–1.77 (m, 4H), 1.27 (s, 9H). ESI-MS m/z 408 ($\text{M} - \text{H}$) $^-$.

(*S*)-1-[2'-(*tert*-Butoxycarbonylamino)-2'-carboxyethyl]thieno[2,3-*d*]pyrimidin-2,4-dione (**12c**). Starting from **11c**, the title compound was prepared following the same procedure described for the synthesis of **12a** and was obtained as a white amorphous solid (yield 18%). $^1\text{H NMR}$ (CD_3OD) δ 7.22 (d, 1H, $J = 5.7$ Hz), 7.09 (d, 1H, $J = 5.7$ Hz), 4.77–4.00 (m, 3H), 1.25 (s, 9H). ESI-MS m/z 354 ($\text{M} - \text{H}$) $^-$.

(*S*)-1-(2'-Amino-2'-carboxyethyl)thieno[3,4-*d*]pyrimidin-2,4-dione (**6a**). To a suspension of **12a** (97 mg, 0.27 mmol) in DCM (10 mL), TFA (2 mL) was added dropwise at 0 °C, and the solution was stirred at rt for 3 h. Then the volatiles were evaporated, and the resulting crude was purified by means of ion-exchange resin (Dowex 50 WX 8-400), using a mixture water/EtOH 1:1 v/v as eluent first, and then diluted NH_3 in water to recover displaced **6a** from the resin. **6a** was obtained as a white amorphous solid (yield 82%); $[\alpha]_D^{20} = +30.5^\circ$ (c 0.1, HCl 6N). $^1\text{H NMR}$ (DCI 20 wt % in D_2O) δ 8.19 (d, 1H, $J = 3.0$ Hz), 6.91 (d, 1H, $J = 3.0$ Hz), 4.45–4.25 (m, 3H). $^{13}\text{C NMR}$ (DCI 20 wt % in D_2O) δ 169.1, 160.0, 152.4, 137.8, 132.7, 121.3, 105.1, 51.3, 44.3. ESI-MS m/z 256 ($\text{M} + \text{H}$) $^+$. HRMS (ESI) m/z calculated for $\text{C}_9\text{H}_{10}\text{N}_3\text{O}_4\text{S}^+$ ($\text{M} + \text{H}$) $^+$ 256.0387, found 256.0390. Anal. ($\text{C}_9\text{H}_9\text{N}_3\text{O}_4\text{S}$) C, H, N.

(*S*)-1-(2'-Amino-2'-carboxyethyl)-1,2,3,4,5,6,7,8-octahydrobenzo[4,5]thieno[2,3-*d*]pyrimidin-2,4-dione (**6b**). Starting from **12b**, the title compound was prepared following the same procedure used for the synthesis of **6a** and was obtained as a white amorphous solid (yield 91%); $[\alpha]_D^{20} = +40.0^\circ$ (c 0.1, HCl 6N). $^1\text{H NMR}$ (DCI 20 wt % in D_2O) δ 4.25–4.15 (m, 2H), 4.06–3.99 (m, 1H), 2.30 (m, 4H), 1.42–1.38 (m, 4H). $^{13}\text{C NMR}$ (DCI 20 wt % in D_2O) δ 168.5, 160.1, 152.8, 151.4, 132.7, 129.2, 114.4, 51.1, 47.0, 24.9, 23.9, 22.3, 21.3. ESI-MS m/z 310 ($\text{M} + \text{H}$) $^+$. HRMS (ESI) m/z calculated for $\text{C}_{13}\text{H}_{16}\text{N}_3\text{O}_4\text{S}^+$ ($\text{M} + \text{H}$) $^+$ 310.0856, found 310.0854. Anal. ($\text{C}_{13}\text{H}_{15}\text{N}_3\text{O}_4\text{S}$) C, H, N.

(*S*)-1-(2'-Amino-2'-carboxyethyl)thieno[2,3-*d*]pyrimidin-2,4-dione (**6c**). Starting from **12c**, the title compound was prepared following the same procedure described for the synthesis of **6a** and was obtained as a white amorphous solid (yield 89%); $[\alpha]_D^{20} = +46.7^\circ$ (c 0.1, HCl 6N). $^1\text{H NMR}$ (DCI 20 wt % in D_2O) δ 6.98 (d, 1H, $J = 5.5$ Hz), 6.90 (d, 1H, $J = 5.5$ Hz), 4.38–4.15 (m, 3H). $^{13}\text{C NMR}$ (DCI 20 wt % in D_2O) δ 168.7, 167.2, 155.0, 152.5, 122.9, 119.1, 116.5, 51.2, 47.6. ESI-MS m/z 256 ($\text{M} + \text{H}$) $^+$. HRMS (ESI) m/z calculated for $\text{C}_9\text{H}_{10}\text{N}_3\text{O}_4\text{S}^+$ ($\text{M} + \text{H}$) $^+$ 256.0387, found 256.0391. Anal. ($\text{C}_9\text{H}_9\text{N}_3\text{O}_4\text{S}$) C, H, N.

Diethyl 3-Methylthiophen-2-phosphonate (**14**). Method A. A suspension of **13** (4.7 g, 26.6 mmol) and Mg turnings (671 mg, 27.9 mmol) in dry THF (30 mL) was refluxed until the formation of the Grignard reagent was completed. Then the obtained clear solution was cooled to 0 °C, and a solution of diethyl chlorophosphate (4.6 g, 26.6 mmol) in dry THF (10 mL) was added dropwise. The resulting mixture was warmed to rt and refluxed for 2 h. Then the reaction mixture was cooled to 0 °C and quenched by addition of water (10 mL) and HCl 1N (10 mL). The aqueous phase was extracted with chloroform (3 \times 50 mL) and the combined organic layers were dried, filtered, and evaporated. The crude product was purified by means of flash chromatography (*n*-hexane/EtOAc, 1:1) to give **14** as a yellow oil (yield 59%).

Method B (Tavs method). A mixture of **13** (200 mg, 1.13 mmol) and $\text{NiCl}_2 \cdot 6\text{H}_2\text{O}$ (268 mg, 1.13 mmol) in triethyl phosphite (2 mL, 11.6 mmol) was heated at 160 °C for 18 h. Then the formed precipitate was filtered through Celite, the volatiles were evaporated, and the crude product was purified by means of flash chromatography (*n*-hexane/EtOAc, 1:1) to give **14** as a yellow oil (yield 45%).

$^1\text{H NMR}$ (CDCl_3) δ 7.46 (m, 1H), 6.92 (m, 1H), 4.14–3.98 (m, 4H), 2.41 (s, 3H), 1.27 (t, 6H, $J = 7.0$ Hz). ESI-MS m/z 257 ($\text{M} + \text{Na}$) $^+$.

Diethyl 3-Bromomethylthiophen-2-phosphonate (**15b**). To a solution of **14** (3.7 g, 11.8 mmol) in CCl_4 (200 mL), *N*-bromosuccinimide (2.1 g, 11.8), and AIBN (195 mg, 1.12 mmol) were added, and the resulting suspension was refluxed for 4 h. Then the precipitate was filtered off, and the solvent was evaporated. The crude was purified by means of flash chromatography (*n*-hexane/EtOAc, 3:1) to furnish **15b** as a yellow oil (yield 82%). $^1\text{H NMR}$ (CDCl_3) δ 7.57 (m, 1H), 7.19 (m, 1H), 4.73 (s, 2H), 4.19–4.03 (m, 4H), 1.3 (t, 6H, $J = 7.0$ Hz). ESI-MS m/z 335 ($\text{M} + \text{Na}$) $^+$.

tert-Butyl 3-Azidomethylthiophen-2-carboxylate (**16a**). To a solution of **15a** (3.9 g, 14.1 mmol) in DMF (30 mL), NaN_3 (1.1 g, 17.0 mmol) was added portionwise and the mixture was stirred at 110 °C for 2 h. The solvent was evaporated and water (25 mL) was added to the residue. The aqueous phase was extracted with chloroform (3 \times 30 mL), and the collected organic layers were dried, filtered, and concentrated. The crude product was purified by means of flash chromatography (*n*-hexane/EtOAc, 50:1) to furnish **16a** as a yellow oil (yield 73%). $^1\text{H NMR}$ (CDCl_3) δ 7.43 (d, 1H, $J = 5.2$ Hz), 7.10 (d, 1H, $J = 5.2$ Hz), 4.71 (s, 2H), 1.57 (s, 9H). ESI-MS m/z 262 ($\text{M} + \text{Na}$) $^+$.

Diethyl 3-Azidomethylthiophen-2-phosphonate (**16b**). Starting from **15b** and following the same procedure described for the synthesis of **16a**, the title compound was obtained as a yellow oil (yield 97%). $^1\text{H NMR}$ (CDCl_3) δ 7.62 (m, 1H), 7.18 (m, 1H), 4.59 (s, 2H), 4.16–4.06 (m, 4H), 1.30 (t, 6H, $J = 7.0$ Hz). ESI-MS m/z 298 ($\text{M} + \text{Na}$) $^+$.

tert-Butyl 3-Aminomethylthiophen-2-carboxylate (**17a**). A suspension of **16a** (2.3 g, 9.8 mmol) and a catalytic amount of Pd/C in THF (80 mL) was stirred under hydrogen atmosphere at 1 atm for 2 h. Then Pd/C was filtered off, and the solvent was evaporated. The crude product was purified by means of flash chromatography (from chloroform/MeOH, 20:1 to 5:1) to give **17a** as a yellow oil (yield 65%). $^1\text{H NMR}$ (CDCl_3) δ 7.36 (d, 1H, $J = 4.9$ Hz), 7.05 (d, 1H, $J = 4.9$ Hz), 4.05 (s, 2H), 1.94 (br s, 2H), 1.56 (s, 9H). ESI-MS m/z 214 ($\text{M} + \text{H}$) $^+$.

Diethyl 3-Aminomethylthiophen-2-phosphonate (**17b**). Starting from **16b** and following the same procedure described for the synthesis of **17a**, the title compound was obtained as a yellow oil (yield 90%). $^1\text{H NMR}$ (CDCl_3) δ 7.50 (m, 1H), 7.12 (m, 1H), 4.10–4.02 (m, 4H), 3.95 (s, 2H), 2.01 (br s, 2H), 1.25 (t, 6H, $J = 7.0$ Hz). ESI-MS m/z 250 ($\text{M} + \text{H}$) $^+$.

tert-Butyl 3-[(3-(4-(Methoxycarbonyl)thiophen-3-yl)ureido)methyl]thiophen-2-carboxylate (**18a**). To a solution of **8a** (400 mg, 2.54 mmol) in dry toluene (20 mL), triphosgene (250 mg, 0.84 mmol) was added and the resulting mixture was refluxed for 3 h. Then the solvent was evaporated, the residue was dissolved in 15 mL of dry toluene, and a solution of **17a** (541 mg, 2.54 mmol) in dry toluene (10 mL) was added, and the resulting mixture was refluxed for further 3 h. Then the solvent was evaporated, and the crude product was purified by means of flash chromatography (*n*-hexane/EtOAc, 5:1) to give **18a** as a white solid (yield 78%). $^1\text{H NMR}$ ($\text{DMSO}-d_6$) δ 9.03 (br s, 1H), 8.27 (d, 1H, $J = 3.5$ Hz), 7.92 (t, 1H, $J = 5.8$ Hz), 7.73 (d, 1H, $J = 5.2$ Hz), 7.64 (d, 1H, $J = 3.5$ Hz), 7.09 (d, 1H, $J = 5.2$ Hz), 4.53 (d, 2H, $J = 5.8$ Hz), 3.81 (s, 3H), 1.52 (s, 9H). ESI-MS m/z 419 ($\text{M} + \text{Na}$) $^+$.

Methyl 3-[(2-(*tert*-Butoxycarbonyl)thiophen-3-yl)methyl]ureido]thiophen-2-carboxylate (**18b**). Starting from methyl 2-aminothiophene-3-carboxylate and **17a**, and following the same procedure used for the synthesis of **18a**, the title compound was obtained as a white solid (yield 96%). $^1\text{H NMR}$ ($\text{DMSO}-d_6$) δ 9.34 (br s, 1H), 8.15 (t, 1H, $J = 5.8$ Hz), 7.91 (d, 1H, $J = 5.5$ Hz), 7.78–7.73 (m, 2H), 7.09 (d, 1H, $J = 5.2$ Hz), 4.54 (d, 2H, $J = 5.8$ Hz), 3.80 (s, 3H), 1.52 (s, 9H). ESI-MS m/z 419 ($\text{M} + \text{Na}$) $^+$.

Diethyl 3-[(3-(4-(Methoxycarbonyl)thiophen-3-yl)ureido)methyl]thiophen-2-phosphonate (**18c**). Starting from **8a** and **17b**, and following the same procedure described for the synthesis of **18a**, the title compound was obtained as a white solid (yield 35%). $^1\text{H NMR}$ ($\text{DMSO}-d_6$) δ 9.03 (br s, 1H), 8.27 (d, 1H, $J = 3.5$ Hz), 7.95 (t, 1H, $J = 5.8$ Hz),

7.73 (m, 1H), 7.64 (d, 1H, $J = 3.5$ Hz), 7.06 (m, 1H), 4.43 (d, 2H, $J = 5.8$ Hz), 4.08–3.95 (m, 4H), 3.82 (s, 3H), 1.23 (t, 6H, $J = 7.0$ Hz). ESI-MS m/z 455 ($M + Na$)⁺.

Diethyl 3-[(3-(2-(Methoxycarbonyl)thiophen-3-yl)ureido)methyl]thiophen-2-phosphonate (**18d**). Starting from methyl 2-aminothiophene-3-carboxylate and **17b**, and following the same procedure used for the synthesis of **18a**, the title compound was obtained as a white solid (yield 73%). ¹H NMR (DMSO-*d*₆) δ 9.33 (br s, 1H), 8.14 (t, 1H, $J = 5.3$ Hz), 7.93–7.90 (m, 2H), 7.77 (d, 1H, $J = 5.5$ Hz), 7.02 (m, 1H), 4.45 (d, 2H, $J = 5.2$ Hz), 4.08–3.97 (m, 4H), 3.79 (s, 3H), 1.23 (t, 6H, $J = 7.0$ Hz). ESI-MS m/z 455 ($M + Na$)⁺.

3-[(2-Carboxythien-3-yl)methyl]thieno[3,4-*d*]pyrimidin-2,4-dione (**19a**). A mixture of **18a** (470 mg, 1.2 mmol) and TFA (4 mL) in DCM (20 mL) was stirred at rt for 3 h. Then the solvent was evaporated, the residue was suspended in 15 mL of MeOH, and 4 mL of NaOH 2N were added. The resulting mixture was refluxed for 1 h. Then MeOH was evaporated, water (8 mL) was added to the residue, and the solution was cooled to 0 °C, acidified with HCl 4N, and the formed solid filtered and dried in oven at 60 °C to give **19a** as a white solid (yield 69%). ¹H NMR (DMSO-*d*₆) δ 13.16 (br s, 1H), 11.99 (br s, 1H), 8.09 (d, 1H, $J = 4.9$ Hz), 7.67 (d, 1H, $J = 4.9$ Hz), 6.95 (d, 1H, $J = 5.2$ Hz), 6.74 (d, 1H, $J = 5.2$ Hz), 5.31 (s, 2H). ESI-MS m/z 307 ($M - H$)⁻.

3-[(2-Carboxythien-3-yl)methyl]thieno[3,2-*d*]pyrimidin-2,4-dione (**19b**). To a solution of **18b** (782 mg, 1.97 mmol) in THF (20 mL) cooled to 0 °C, sodium *tert*-butoxide (480 mg, 4.98 mmol) was added, and the resulting suspension was stirred for 1 h at rt. Then the solvent was evaporated, the residue was dissolved in 10 mL of water, and the solution was cooled to 0 °C and acidified by addition of HCl 4N. The formed precipitate was filtered, washed with water and MeOH, and dried in oven at 60 °C to give **19b** as a white solid (yield 76%). ¹H NMR (DMSO-*d*₆) δ 13.16 (br s, 1H), 11.34 (br s, 1H), 8.40 (d, 1H, $J = 3.2$ Hz), 7.44 (d, 1H, $J = 5.2$ Hz), 6.87 (d, 1H, $J = 3.2$ Hz), 6.61 (d, 1H, $J = 5.2$ Hz), 5.31 (m, 2H). ESI-MS m/z 307 ($M - H$)⁻.

Methyl 4-(6,8-Dioxo-5,6-dihydro-4H-thieno[3,2-*e*][1,3]diazepin-7(8H)-yl)thiophen-3-carboxylate (**20**). The title compound was obtained as byproduct in the synthesis of **19b**. The methanol acidic solution, from which **19b** was precipitated, and the methanol layers used to wash **19b** were collected and concentrated. The residue was purified by means of flash chromatography (EtOAc/MeOH, 4:1) to give **20** as a white solid (yield 15%). ¹H NMR (DMSO-*d*₆) δ 11.35 (br s, 1H), 8.41 (d, 1H, $J = 2.6$ Hz), 7.73 (d, 1H, $J = 3.2$ Hz), 6.87 (d, 1H, $J = 2.6$ Hz), 6.79 (d, 1H, $J = 3.2$ Hz), 5.28 (s, 2H), 3.83 (s, 3H). ESI-MS m/z 345 ($M + Na$)⁺.

3-[(2-Diethylphosphonothien-3-yl)methyl]thieno[3,4-*d*]pyrimidin-2,4-dione (**19c**). To a freshly prepared 5N NaOEt solution (20 mL), **18c** (688 mg, 1.59 mmol) was added and the suspension was stirred at rt for 3 h. Then the solvent was evaporated and the residue was taken up with water (10 mL). The solution was cooled to 0 °C and acidified by dropwise addition of HCl 4N. The obtained precipitate was recovered by filtration and dried in oven at 60 °C to give **19c** as a white solid (yield, 99%). ¹H NMR (DMSO-*d*₆) δ 11.33 (br s, 1H), 8.41 (d, 1H, $J = 3.2$ Hz), 7.83 (m, 1H), 6.88–6.83 (m, 2H), 5.17 (s, 2H), 4.11–4.02 (m, 4H), 1.26 (t, 6H, $J = 7.0$ Hz). ESI-MS m/z 423 ($M + Na$)⁺.

3-[(2-Diethylphosphonothien-3-yl)methyl]thieno[3,2-*d*]pyrimidin-2,4-dione (**19d**). Starting from **18d** and following the same procedure described for **19c**, the title compound was obtained as a white solid (yield 99%). ¹H NMR (DMSO-*d*₆) δ 11.97 (br s, 1H), 8.09 (d, 1H, $J = 5.2$ Hz), 7.84 (m, 1H), 6.95 (d, 1H, $J = 5.2$ Hz), 6.83 (m, 1H), 5.19 (s, 2H), 4.09–4.02 (m, 4H), 1.25 (t, 6H, $J = 7.0$ Hz). ESI-MS m/z 423 ($M + Na$)⁺.

(*S*)-1-[2'-(*tert*-Butoxycarbonylamino)-2'-carboxyethyl]-3-[(2-carboxythien-3-yl)methyl]thieno[3,4-*d*]pyrimidin-2,4-dione (**21a**). Starting from **19a**, and following the same procedure used for the synthesis of **12a**, the title compound was obtained as a white amorphous solid (yield 19%). ¹H NMR (CD₃OD) δ 8.34 (d, 1H, $J = 3.2$ Hz), 7.47 (d, 1H,

$J = 5.2$ Hz), 7.19 (d, 1H, $J = 3.2$ Hz), 6.96 (d, 1H, $J = 5.2$ Hz), 5.60–5.43 (m, 2H), 4.69–4.12 (m, 3H), 1.22 (s, 9H). ESI-MS m/z 494 ($M - H$)⁻.

(*S*)-1-[2'-(*tert*-Butoxycarbonylamino)-2'-carboxyethyl]-3-[(2-carboxythien-3-yl)methyl]thieno[3,2-*d*]pyrimidin-2,4-dione (**21b**). Starting from **19b**, and following the same procedure used for the synthesis of **12a**, the title compound was obtained as a white amorphous solid (yield 38%). ¹H NMR (CD₃OD) δ 7.98 (d, 1H, $J = 5.2$ Hz), 7.46 (d, 1H, $J = 5.2$ Hz), 7.34 (d, 1H, $J = 5.2$ Hz), 7.01 (d, 1H, $J = 5.2$ Hz), 5.65–5.46 (m, 2H), 4.71–4.65 (m, 2H), 4.16 (m, 1H), 1.22 (s, 9H). ESI-MS m/z 494 ($M - H$)⁻.

(*S*)-1-[2'-(*tert*-Butoxycarbonylamino)-2'-carboxyethyl]-3-[(2-diethylphosphonothien-3-yl)methyl]thieno[3,4-*d*]pyrimidin-2,4-dione (**21c**). Starting from **19c**, and following the same procedure described for **12a** (but using only 1.56 mmol of NaH), the title compound was obtained as a white amorphous solid (yield 38%). ¹H NMR (CD₃OD) δ 8.34 (d, 1H, $J = 3.2$ Hz), 7.71 (m, 1H), 7.19 (d, 1H, $J = 3.2$ Hz), 7.11 (m, 1H), 5.39–5.36 (m, 2H), 4.76–4.50 (m, 2H), 4.25–4.12 (m, 5H), 1.33 (t, 6H, $J = 7.0$ Hz), 1.24 (s, 9H). ESI-MS m/z 586 ($M - H$)⁻.

(*S*)-1-[2'-(*tert*-Butoxycarbonylamino)-2'-carboxyethyl]-3-[(2-diethylphosphonothien-3-yl)methyl]thieno[3,2-*d*]pyrimidin-2,4-dione (**21d**). Starting from **19d**, and following the same procedure described for **21c**, the title compound was obtained as a white amorphous solid (yield 45%). ¹H NMR (CD₃OD) δ 7.99 (d, 1H, $J = 5.2$ Hz), 7.72 (m, 1H), 7.34 (d, 1H, $J = 5.2$ Hz), 7.16 (m, 1H), 5.47–5.45 (m, 2H), 4.74–4.44 (m, 2H), 4.24–4.15 (m, 5H), 1.38 (t, 6H, $J = 7.0$ Hz), 1.23 (s, 9H). ESI-MS m/z 586 ($M - H$)⁻.

(*S*)-1-[2'-(*tert*-Amino-2'-carboxyethyl)-3-[(2-carboxythien-3-yl)methyl]thieno[3,4-*d*]pyrimidin-2,4-dione (**7a**). Starting from **21a**, and following the same procedure used for the synthesis of **6a**, the title compound was obtained as a white solid (yield 98%); [α]_D²⁰ = +29.1° (*c* 0.72, HCl 6N). ¹H NMR (D₂O) δ 8.27 (d, 1H, $J = 3.2$ Hz), 7.22 (d, 1H, $J = 5.2$ Hz), 7.01 (d, 1H, $J = 3.2$ Hz), 6.65 (d, 1H, $J = 5.2$ Hz), 5.31 (m, 2H), 4.46–4.26 (m, 2H), 4.04 (m, 1H). ¹³C NMR (D₂O) δ 171.6, 159.8, 152.7, 139.8, 136.9 (2C), 136.0, 132.6, 128.6, 127.4, 121.1, 104.7, 53.6, 46.7, 41.3. ESI-MS m/z 394 ($M - H$)⁻. HRMS (ESI) m/z calculated for C₁₅H₁₂N₃O₆S₂⁻ ($M - H$)⁻ 394.0173, found 394.0175. Anal. (C₁₅H₁₃N₃O₆S₂) C, H, N.

(*S*)-1-[2'-(*tert*-Amino-2'-carboxyethyl)-3-[(2-carboxythien-3-yl)methyl]thieno[3,2-*d*]pyrimidin-2,4-dione (**7b**). Starting from **21b**, and following the same procedure used for the synthesis of **6a**, the title compound was obtained as a white solid (yield 95%); [α]_D²⁰ = +20.5° (*c* 0.14, HCl 6N). ¹H NMR (D₂O) δ 7.55 (d, 1H, $J = 5.2$ Hz), 7.05 (d, 1H, $J = 5.2$ Hz), 6.73 (d, 1H, $J = 5.2$ Hz), 6.30 (d, 1H, $J = 5.2$ Hz), 4.92–4.78 (m, 2H), 4.14–4.02 (m, 3H). ¹³C NMR (D₂O) δ 168.5, 165.1, 159.5, 152.8, 145.6, 144.2, 137.9, 132.6, 127.6, 126.8, 116.5, 113.0, 51.3, 46.0, 41.3. ESI-MS m/z 394 ($M - H$)⁻. HRMS (ESI) m/z calculated for C₁₅H₁₂N₃O₆S₂⁻ ($M - H$)⁻ 394.0173, found 394.0170. Anal. (C₁₅H₁₃N₃O₆S₂) C, H, N.

(*S*)-1-[2'-(*tert*-Amino-2'-carboxyethyl)-3-[(2-phosphonothien-3-yl)methyl]thieno[3,4-*d*]pyrimidin-2,4-dione (**7c**). To a suspension of **21c** (200 mg, 0.34 mmol) in DCM (15 mL), bromotrimethylsilane (900 μ L, 6.8 mmol) was added and the mixture was refluxed for 18 h. Then the volatiles were evaporated and crude product was purified by means of Dowex resin as described for **6a** to give **7c** as a white solid (yield 91%); [α]_D²⁰ = +25.0° (*c* 0.2, H₂O). ¹H NMR (D₂O) δ 8.28 (d, 1H, $J = 3.2$ Hz), 7.29 (m, 2H), 7.01 (d, 1H, $J = 3.2$ Hz), 5.22–5.19 (m, 2H), 4.49–4.26 (m, 2H), 4.04–4.00 (m, 1H). ¹³C NMR (D₂O) δ 171.6, 159.9, 152.8, 140.2 (JC–P = 9.9 Hz), 137.0, 132.9 (JC–P = 18.1 Hz), 132.6, 128.9 (JC–P = 6.7 Hz), 127.5 (JC–P = 14.9 Hz), 121.2, 104.7, 53.7, 46.7, 41.6. ³¹P NMR (D₂O) δ 4.92. ESI-MS m/z 432 ($M + H$)⁺, 430 ($M - H$)⁻. HRMS (ESI) m/z calculated for C₁₄H₁₃N₃O₇PS₂⁻ ($M - H$)⁻ 429.9938, found 429.9942. Anal. (C₁₄H₁₄N₃O₇PS₂) C, H, N.

(*S*)-1-[2'-(*tert*-Amino-2'-carboxyethyl)-3-[(2-phosphonothien-3-yl)methyl]thieno[3,2-*d*]pyrimidin-2,4-dione (**7d**). Starting from **21d**, and following the same procedure used for the synthesis of **7c**, the title compound

was obtained as a white solid (yield 89%); $[\alpha]_D^{20} = +40.0^\circ$ (c 0.1, H₂O). ¹H NMR (D₂O) δ 7.94 (d, 1H, $J = 5.2$ Hz), 7.31 (m, 1H), 7.16 (d, 1H, $J = 5.2$ Hz), 6.69–6.66 (m, 1H), 5.30–5.18 (m, 2H), 4.51–4.44 (m, 2H), 4.02–3.98 (m, 1H). ¹³C NMR (D₂O) δ 171.4, 160.2, 153.5, 146.2, 139.4 ($J_{C-P} = 9.9$ Hz), 137.5, 133.9 ($J_{C-P} = 181.3$ Hz), 128.7 ($J_{C-P} = 6.6$ Hz), 127.1 ($J_{C-P} = 14.8$ Hz), 117.0, 113.2, 54.1, 47.3, 41.9. ESI-MS m/z 432 (M + H)⁺, 430 (M – H)[–]. HRMS (ESI) m/z calculated for C₁₄H₁₃N₃O₇PS₂[–] (M – H)[–] 429.9938, found 429.9940. Anal. (C₁₄H₁₄N₃O₇PS₂) C, H, N.

Molecular Modeling. *Docking Calculations.* Selected compounds were docked into the GluA2 and GluK1 receptor by means of AUTODOCK 4.0 program. Docking simulations of the compounds were carried out by means of the Lamarckian Genetic Algorithm and applying a protocol with an initial population of 50 randomly placed individuals, a maximum number of 25×10^6 energy evaluations, a mutation rate of 0.02, a crossover rate of 0.80, and an elitism value of 1. The pseudo-Solis and Wets algorithm with a maximum of 300 interactions was applied for the local search. Two hundred independent docking runs were carried out for each ligand, and the resulting conformations which differ by less than 1.0 Å in positional root-mean-square deviation (rmsd) were clustered together. The conformer with the lowest free energy of binding was taken as the representative of the most populated cluster.

Ligand Set up. The structures of the ligands were generated by means of MacMolPlt³² program starting from the X-ray data. Geometry optimizations were achieved by means of 100 steps of the RHF 6-31G* basis set as implemented GAMESS program.³³ Partial atomic charges were calculated by means of ab initio methods and then used for docking conformational space.

Protein Set up. The receptor model was set up for docking as follows: water molecules were removed, polar hydrogens were added by means of AutoDockTools software and united-atom partial charges were assigned. ADDSOL utility of the AutoDock program was used to add solvation parameters to the protein structures and the grid maps representing the proteins in the docking process were calculated by means of AutoGrid. The grids, one for each atom type in the ligand, plus one for electrostatic interactions, were chosen to be large enough to include not only the hypothetical binding site, but also a significant part of the protein around it. As a consequence, for all docking calculations, the dimensions of grid map was 56 Å × 54 Å × 60 Å for GluA2 and 70 Å × 66 Å × 102 Å for GluK1 with a grid-point spacing of 0.375 Å.

Molecular Electrostatic Potential Calculations. For compounds 3, 4, and 6b, the electrostatic potential was calculated by means of GAMESS and mapped on the electron density surface. Electrostatic potential was computed using Hartree–Fock functional and 6-31G* basis set. Results were visualized by means of MacMolPlt program.

Radioligand Binding Assay. Drug affinities at cloned rat iGluR were determined as previously described.³⁴

Two Electrode Voltage Clamp (TEVC) Electrophysiology. *X. laevis* oocytes were collected, prepared, injected, and maintained as previously described.³⁵ TEVC electrophysiology was carried out as previously described³⁵ on nondesensitizing mutants of GluK1–3.³¹ Agonist concentration–response data were fit to the logistic equation: $I = I_{\max}/(1 + (10^{(\log EC_{50} - \log [A])})^{n_H})$. Antagonist concentration–response data were fit to the logistic equation: $I = I_{\max}/(1 + (10^{(\log [B] - \log IC_{50})})^{n_H}) + \text{baseline}$; where I is the agonist-evoked current, $[A]$ is the agonist concentration, $[B]$ is the antagonist concentration, I_{\max} is the maximal response in the absence of antagonist, EC_{50} is the concentration of the agonist giving 50% maximal response, IC_{50} is the concentration of the antagonist giving 50% inhibition, n_H is the Hill coefficient, and baseline represents any baseline current that is blocked by antagonist. (S)-Glutamate was used as the agonist (100 μM at GluK1 and GluK2; 5 or 10 mM at GluK3; $EC_{50} = 83.5$ μM, 108 μM, and 9.03 mM, respectively) in antagonist concentration–response experiments. K_b values were calculated from the IC_{50} values using the modified Cheng–Prusoff equation.³⁶ Data were

collected using WinWCP software (Strathclyde University, Glasgow, Scotland) and concentration response curves fitted using GraFit (Erithacus Software Ltd., UK). Statistical analysis of data was performed using SigmaPlot v11 (Systat Software Inc., San Jose, CA).

Crystallization. The rat GluK1 LBD (GluK1-S1S2) was prepared and purified as previously described.³⁷ Crystallization of the GluK1 LBD with 7a was carried out using the hanging drop vapor diffusion method at 6 °C. The protein–7a solution consisted of 6.2 mg/mL GluK1 LBD, 4.6 mM 7a, 20 mM NaCl, 1 mM EDTA, and 10 mM HEPES pH 7.0. The drops contained 1 μL of protein–7a solution and 1 μL of reservoir solution. The reservoir volume was 0.5 mL. Crystals were obtained with a reservoir solution containing 24.4% PEG4000, 0.3 M lithium sulfate, 0.1 M phosphate-citrate pH 4.5.

Data Collection and Processing. Crystals were flash frozen in liquid nitrogen, after soaking them into cryo buffer consisting of reservoir solution with 20% glycerol. X-ray data were collected to 2.5 Å resolution at the I911-3 beamline (MAX-Lab, Lund, Sweden). Data processing was performed using XDS³⁸ and the CCP4 suite of programs.³⁹ Structure determination was carried out by molecular replacement, using Phaser⁴⁰ implemented in CCP4. The GluK1 LBD structure in complex with 5 (PDB code 2F34, molA) was used as search model. Further model building was performed by tracing amino acid residues with ARP/wARP⁴¹ within CCP4. Some residues that could not be built in automatically were added manually using program COOT.⁴² Coordinate and molecular restraint files for the 7a compound were generated using the ProDrg server.⁴³ The structure was refined using Phenix.⁴⁴ Between the refinements, COOT was used to check and correct the model. The 7a compound, water molecules, glycerol, sulfate, and chloride ions were manually modeled into the electron density.

Structure Analysis. Ligand–7a interactions were analyzed and distances measured in COOT. Domain openings were calculated using the DynDom server.⁴⁵ Figures were prepared using PyMol⁴⁶ and MOE.²⁶

■ ASSOCIATED CONTENT

S Supporting Information. Crystallography data, elemental analyses for final compounds. This material is available free of charge via the Internet at <http://pubs.acs.org>.

Accession Codes

[†]Coordinates have been deposited in the RCSB Protein Data Bank under accession code 3S2V.

■ AUTHOR INFORMATION

Corresponding Author

*Phone: 0039-0577-234161. Fax: 0039-0577-234333. E-mail: butini3@unisi.it.

■ ACKNOWLEDGMENT

Technician Heidi Peterson is thanked for preparation of GluK1 soluble protein and MAX-lab, Lund, Sweden, for allocation of beamtime. We thank NatSynDrugs, MIUR (PRIN), Danscatt, and GluTarget for financial support.

■ ABBREVIATIONS USED

Glu, Glutamate; iGluRs, ionotropic Glu receptors; KARs, kainate receptors; AMPA, (S)-2-amino-3-(5-methyl-3-hydroxyisoxazol-4-yl)propanoic acid; NMDA, N-methyl-D-aspartate; CNS, central nervous system; DRG, dorsal root ganglia; GABA, γ -aminobutyric acid; SARs, structure–activity relationships; LBD, ligand

binding domain; (S)-CPW399, (S)-1-(2-amino-2-carboxyethyl)-6,7-dihydro-1H-cyclopenta[d]pyrimidin-2,4(1H,3H)dione; vdW, van der Waals; TEVC, two electrode voltage clamp

REFERENCES

- (1) Meldrum, B. S. Glutamate as a neurotransmitter in the brain: review of physiology and pathology. *J. Nutr.* **2000**, *130*, 1007S–1015S.
- (2) Lerma, J. Kainate receptor functions. In *Encyclopedia of Neuroscience*; Elsevier Ltd.: New York, 2009.
- (3) Pinheiro, P. S.; Perrais, D.; Coussen, F.; Barhanin, J.; Bettler, B.; Mann, J. R.; Malva, J. O.; Heinemann, S. F.; Mulle, C. GluR7 is an essential subunit of presynaptic kainate autoreceptors at hippocampal mossy fiber synapses. *Proc. Natl. Acad. Sci. U.S.A.* **2007**, *104*, 12181–12186.
- (4) Sobolevsky, A. I.; Rosconi, M. P.; Gouaux, E. X-ray structure, symmetry and mechanism of an AMPA-subtype glutamate receptor. *Nature* **2009**, *462*, 745–756.
- (5) Huettner, J. E. Kainate receptors and synaptic transmission. *Prog. Neurobiol.* **2003**, *70*, 387–407.
- (6) Jane, D. E.; Lodge, D.; Collingridge, G. L. Kainate receptors: pharmacology, function and therapeutic potential. *Neuropharmacology* **2009**, *56*, 90–113.
- (7) Lerma, J. Kainate receptor physiology. *Curr. Opin. Pharmacol.* **2006**, *6*, 89–97.
- (8) Bleakman, D. Kainate receptor pharmacology and physiology. *Cell. Mol. Life Sci.* **1999**, *56*, 558–566.
- (9) Bleakman, D.; Alt, A.; Nisenbaum, E. S. Glutamate receptors and pain. *Semin. Cell Dev. Biol.* **2006**, *17*, 592–604.
- (10) Smolders, I.; Bortolotto, Z. A.; Clarke, V. R.; Warre, R.; Khan, G. M.; O'Neill, M. J.; Ornstein, P. L.; Bleakman, D.; Ogdan, A.; Weiss, B.; Stables, J. P.; Ho, K. H.; Ebinger, G.; Collingridge, G. L.; Lodge, D.; Michotte, Y. Antagonists of GLU(K5)-containing kainate receptors prevent pilocarpine-induced limbic seizures. *Nature Neurosci.* **2002**, *5*, 796–804.
- (11) Larsen, A. M.; Bunch, L. Medicinal Chemistry of Competitive Kainate Receptor Antagonists. *ACS Chem. Neurosci.* **2010**, *2*, 60–74.
- (12) Jane, D. E.; Hoo, K.; Kamboj, R.; Deverill, M.; Bleakman, D.; Mandelzys, A. Synthesis of willardiine and 6-azawillardiine analogs: pharmacological characterization on cloned homomeric human AMPA and kainate receptor subtypes. *J. Med. Chem.* **1997**, *40*, 3645–3650.
- (13) Dolman, N. P.; Troop, H. M.; More, J. C.; Alt, A.; Knauss, J. L.; Nistico, R.; Jack, S.; Morley, R. M.; Bortolotto, Z. A.; Roberts, P. J.; Bleakman, D.; Collingridge, G. L.; Jane, D. E. Synthesis and pharmacology of willardiine derivatives acting as antagonists of kainate receptors. *J. Med. Chem.* **2005**, *48*, 7867–7881.
- (14) Dolman, N. P.; More, J. C.; Alt, A.; Knauss, J. L.; Troop, H. M.; Bleakman, D.; Collingridge, G. L.; Jane, D. E. Structure–activity relationship studies on N3-substituted willardiine derivatives acting as AMPA or kainate receptor antagonists. *J. Med. Chem.* **2006**, *49*, 2579–2592.
- (15) Dolman, N. P.; More, J. C.; Alt, A.; Knauss, J. L.; Pentikainen, O. T.; Glasser, C. R.; Bleakman, D.; Mayer, M. L.; Collingridge, G. L.; Jane, D. E. Synthesis and pharmacological characterization of N3-substituted willardiine derivatives: role of the substituent at the 5-position of the uracil ring in the development of highly potent and selective GLUK5 kainate receptor antagonists. *J. Med. Chem.* **2007**, *50*, 1558–1570.
- (16) Campiani, G.; Morelli, E.; Nacci, V.; Fattorusso, C.; Ramunno, A.; Novellino, E.; Greenwood, J.; Liljefors, T.; Griffiths, R.; Sinclair, C.; Reavy, H.; Kristensen, A. S.; Pickering, D. S.; Schousboe, A.; Cagnotto, A.; Fumagalli, E.; Mennini, T. Characterization of the 1H-cyclopentapyrimidine-2,4(1H,3H)-dione derivative (S)-CPW399 as a novel, potent, and subtype-selective AMPA receptor full agonist with partial desensitization properties. *J. Med. Chem.* **2001**, *44*, 4501–4504.
- (17) Butini, S.; Pickering, D. S.; Morelli, E.; Coccone, S. S.; Trotta, F.; De Angelis, M.; Guarino, E.; Fiorini, L.; Campiani, G.; Novellino, E.; Schousboe, A.; Christensen, J. K.; Gemma, S. 1H-Cyclopentapyrimidine-2,4(1H,3H)-dione-related ionotropic glutamate receptors ligands. Structure–activity relationships and identification of potent and selective iGluR5 modulators. *J. Med. Chem.* **2008**, *51*, 6614–6618.
- (18) Meyer, M. D.; Altenbach, R. J.; Bai, H.; Basha, F. Z.; Carroll, W. A.; Kerwin, J. F., Jr.; Lebold, S. A.; Lee, E.; Pratt, J. K.; Sippy, K. B.; Tietje, K.; Wendt, M. D.; Brune, M. E.; Buckner, S. A.; Hancock, A. A.; Drizin, I. Structure–activity studies for a novel series of bicyclic substituted hexahydrobenz[e]isoindole alpha1A adrenoceptor antagonists as potential agents for the symptomatic treatment of benign prostatic hyperplasia. *J. Med. Chem.* **2001**, *44*, 1971–85.
- (19) Fossey, H. L.; Laduree, D.; Robba, M. Synthesis of N-1-β-D-arabinosyl and N-1-2'-deoxy-β-D-erythro-pentofuranosyl thieno[3,2-d]-pyrimidine nucleosides. *Nucleosides Nucleotides* **1994**, *4*, 925–937.
- (20) Sun, G.; Uretsky, N. J.; Wallace, L. J.; Shams, G.; Weinstein, D. M.; Miller, D. D. Synthesis of chiral 1-(2'-amino-2'-carboxyethyl)-1,4-dihydro-6,7-quinoxaline-2,3-diones: alpha-amino-3-hydroxy-5-methyl-4-isoxazolepropionate receptor agonists and antagonists. *J. Med. Chem.* **1996**, *39*, 4430–4438.
- (21) Tavs, P. Reaktion von Arylhalogeniden mit trialkylphosphiten und benzolphosphonigsäure-dialkylestern zu aromatischen phosphonsäureestern und phosphinsäureestern unter Nickelsalzkatalyse. *Chem. Ber.* **1970**, *103*, 2428–2436.
- (22) Gerbier, P.; Guerin, C.; Henner, B.; Unal, J. R. An organo-metallic route to zinc phosphonates and their intercalates. *J. Mater. Chem.* **1999**, *9*, 2559–2565.
- (23) Bunger, A.; Dawson, N. D. The reaction of dialkyl chlorophosphates with arylmagnesium halides. *J. Org. Chem.* **1951**, *16*, 1250–1254.
- (24) Atlason, P. T.; Scholefield, C. L.; Eaves, R. J.; Mayo-Martin, M. B.; Jane, D. E.; Molnar, E. Mapping the ligand binding sites of kainate receptors: molecular determinants of subunit-selective binding of the antagonist [3H]UBP310. *Mol. Pharmacol.* **2010**, *78*, 1036–1045.
- (25) Alushin, G. M.; Jane, D.; Mayer, M. L. Binding site and ligand flexibility revealed by high resolution crystal structures of GluK1 competitive antagonists. *Neuropharmacology* **2010**, *60*, 126–134.
- (26) MOE Software, 2006.08; Chemical Computing Group Inc.: Montreal, 2006.
- (27) Mayer, M. L.; Ghosal, A.; Dolman, N. P.; Jane, D. E. Crystal structures of the kainate receptor GluR5 ligand binding core dimer with novel GluR5-selective antagonists. *J. Neurosci.* **2006**, *26*, 2852–2861.
- (28) Mayer, M. L. Crystal structures of the GluR5 and GluR6 ligand binding cores: molecular mechanisms underlying kainate receptor selectivity. *Neuron* **2005**, *45*, 539–552.
- (29) Frandsen, A.; Pickering, D. S.; Vestergaard, B.; Kasper, C.; Nielsen, B. B.; Greenwood, J. R.; Campiani, G.; Fattorusso, C.; Gajhede, M.; Schousboe, A.; Kastrop, J. S. Tyr702 is an important determinant of agonist binding and domain closure of the ligand-binding core of GluR2. *Mol. Pharmacol.* **2005**, *67*, 703–713.
- (30) Perrais, D.; Pinheiro, P. S.; Jane, D. E.; Mulle, C. Antagonism of recombinant and native GluK3-containing kainate receptors. *Neuropharmacology* **2009**, *56*, 131–140.
- (31) Weston, M. C.; Schuck, P.; Ghosal, A.; Rosenmund, C.; Mayer, M. L. Conformational restriction blocks glutamate receptor desensitization. *Nature Struct. Mol. Biol.* **2006**, *13*, 1120–1127.
- (32) Bode, B. M.; Gordon, M. S. MacMolPlt: a graphical user interface for GAMESS. *J. Mol. Graphics Modell.* **1998**, *16* (133–138), 164.
- (33) Baldrige, K. K.; Gordon, M. S.; Jensen, J. H.; Matsunaga, N.; Schmidt, M. W.; Windus, T. L.; Boatz, J. A.; Cundari, T. R. Applications of Parallel GAMESS. In *Parallel Computing in Computational Chemistry*; American Chemical Society: Washington, DC, 1995; Vol. 592, p 29–46.
- (34) Frydenvang, K.; Pickering, D. S.; Greenwood, J. R.; Krogsgaard-Larsen, N.; Brehm, L.; Nielsen, B.; Vogensen, S. B.; Hald, H.; Kastrop, J. S.; Krogsgaard-Larsen, P.; Clausen, R. P. Biostructural and Pharmacological Studies of Bicyclic Analogues of the 3-Isloxazolol Glutamate Receptor Agonist Ibotenic Acid. *J. Med. Chem.* **2010**, *53*, 8354–8361.
- (35) Greenwood, J. R.; Mewett, K. N.; Allan, R. D.; Martin, B. O.; Pickering, D. S. 3-Hydroxypyridazine 1-oxides as carboxylate bioisosteres: a new series of subtype-selective AMPA receptor agonists. *Neuropharmacology* **2006**, *51*, 52–59.

- (36) Leff, P.; Dougall, I. G. Further concerns over Cheng–Prusoff analysis. *Trends Pharmacol. Sci.* **1993**, *14*, 110–112.
- (37) Naur, P.; Vestergaard, B.; Skov, L. K.; Egebjerg, J.; Gajhede, M.; Kastrup, J. S. Crystal structure of the kainate receptor GluR5 ligand-binding core in complex with (S)-glutamate. *FEBS Lett.* **2005**, *579*, 1154–1160.
- (38) Kabsch, W. Xds. *Acta Crystallogr., Sect. D: Biol. Crystallogr.* **2010**, *66*, 125–132.
- (39) The CCP4 suite: programs for protein crystallography. *Acta Crystallogr., Sect. D: Biol. Crystallogr.* **1994**, *50*, 760–763.
- (40) McCoy, A. J.; Grosse-Kunstleve, R. W.; Adams, P. D.; Winn, M. D.; Storoni, L. C.; Read, R. J. Phaser crystallographic software. *J. Appl. Crystallogr.* **2007**, *40*, 658–674.
- (41) Perrakis, A.; Morris, R.; Lamzin, V. S. Automated protein model building combined with iterative structure refinement. *Nature Struct. Biol.* **1999**, *6*, 458–463.
- (42) Emsley, P.; Cowtan, K. Coot: model-building tools for molecular graphics. *Acta Crystallogr., Sect. D: Biol. Crystallogr.* **2004**, *60*, 2126–2132.
- (43) Schuttelkopf, A. W.; van Aalten, D. M. PRODRG: a tool for high-throughput crystallography of protein–ligand complexes. *Acta Crystallogr., Sect. D: Biol. Crystallogr.* **2004**, *60*, 1355–1363.
- (44) Adams, P. D.; Grosse-Kunstleve, R. W.; Hung, L. W.; Ioerger, T. R.; McCoy, A. J.; Moriarty, N. W.; Read, R. J.; Sacchettini, J. C.; Sauter, N. K.; Terwilliger, T. C. PHENIX: building new software for automated crystallographic structure determination. *Acta Crystallogr., Sect. D: Biol. Crystallogr.* **2002**, *58*, 1948–1954.
- (45) Hayward, S.; Lee, R. A. Improvements in the analysis of domain motions in proteins from conformational change: DynDom version 1.50. *J. Mol. Graphics Modell.* **2002**, *21*, 181–183.
- (46) DeLano, L. W. *The PyMOL Molecular Graphics System*; DeLano Scientific: San Carlos CA, 2002.